Modeling edge recombination in silicon solar cells

Andreas Fell, Jonas Schön, Matthias Müller, Nico Wöhrle, Martin C. Schubert and Stefan W. Glunz

Abstract—**A new approach to model edge recombination in silicon solar cells is presented. The model accounts for recombination both at the edge of the quasi-neutral bulk as well as at an exposed space-charge-region (SCR), the latter via an edge-length specific diode property with an ideality factor of 2: a localized $J_{02,edge}$. The model is implemented in Quokka3, where the $J_{02,edge}$ is applied locally to the edges of the 3D geometry, imposing less simplifying assumptions compared to the common way of applying it as an external diode. A "worst-case" value for $J_{02,edge}$, assuming very high surface recombination, is determined by fitting to full detailed device simulations which resolve the SCR recombination. A value of ~19 nA/cm is found, which is shown to be largely independent of device properties. The new approach is applied to model the impact of edge recombination on full-cell performance for a substantial variety of device properties. It is found that recombination at the quasi-neutral bulk edge does not increase the J_{02} of the dark JV-curve, but still shows a non-ideal impact on the light JV-curve similar to the SCR recombination. This needs to be considered in the experimental evaluation of edge losses, which is commonly performed via fitting J_{02} to dark-JV curves.**

Index Terms—**Modeling, solar cell, edge recombination, edge losses, Quokka, simulation, silicon**

I. INTRODUCTION

EDGE losses in silicon solar cells are becoming increasingly important to consider in their development and optimization. On the one hand, the overall decrease of main loss mechanisms is putting non-dominant ones more in focus. On the other hand, high performance module concepts under investigation use cut solar cells with an increased edge-to-area ratio and potentially high edge recombination, like half-cell modules [1, 2] or shingled modules [3–5].

One of the main causes for edge losses is surface recombination at the edge, which is hard to avoid entirely. Other possible causes are e.g. a non-optimal distance between the edge and the finger positions, and a non-illuminated periphery in shingle modules or in-wafer record cells [6–8].

This work investigates the recombination-related edge losses for the common case of an exposed pn-junction bordering the edge.

A widely used and accepted approach to model such edge recombination is to apply an edge-length specific parallel diode with an ideality factor of 2: $J_{02,edge}$ [9] (note its length specific unit of A/cm). This is motivated by theory, as the edge losses are assumed to be dominated by recombination in the space-charge-region (SCR), with approximately equal excess carrier densities, see discussion in [10]. In Fig. 1 a typical simulated surface recombination rate is shown to narrowly peak within the SCR around the point of equal carrier density, supporting this theoretical motivation. In [10], the simulated dark JV-curve of a typical n^+pp^+ structure bordering an edge was found an upper limit for $J_{02,edge}$ of ~20 nA/cm. This is broadly consistent with several published values empirically derived from dark-JV measurements of cells with varying edge-to-area ratio, ranging from 5 nA/cm to 20 nA/cm [3, 9, 11–15], and in few cases up to 70 nA/cm in [9]. In [16] an improved modeling approach was presented by considering the locality of the edge recombination by solving a quasi-2D distributed circuit model representing the full cell geometry.

This work extends on previous works by clarifying some implied assumptions and uncertainties:
  i)   how device properties influence the magnitude of SCR recombination, i.e. $J_{02,edge}$,
  ii) what the influence of the edge recombination outside of the SCR is (i.e. of recombination at the quasi-neutral (qn) bulk edge),
  iii) how for a fixed edge recombination scenario, device properties influence its impact on full-cell performance, and
  iv) whether superposition implied by the external diode model holds for edge recombination, i.e. whether the same losses are observed in the dark-JV and light-JV case, and whether SCR and qn-bulk edge recombination are additive.

Answering above questions accurately via experiments is highly challenging, due to the hard-to-control and -characterize edge properties, the limited influence on the cell's

A. Fell, J. Schön, N. Wöhrle, M. C. Schubert and S. W. Glunz are with the Fraunhofer Institute for Solar Energy Systems, 79110 Freiburg, Germany (e-mail: andreas.fell@ise.fraunhofer.de, jonas.schoen@ise.fraunhofer.de, nico.woehrle@ise.fraunhofer.de, martin.schubert@ise.fraunhofer.de, stefan.glunz@ise.fraunhofer.de).

M. Müller is with the Technical University Bergakademie Freiberg, Institute of Applied Physics, 09599 Freiberg, Germany (e-mail: matth.mueller@physik.tu-freiberg.de).

J. Schön and S. W. Glunz are also with the Department of Sustainable Systems Engineering (INATECH), Albert Ludwigs University of Freiburg, 79110 Freiburg, Germany

characteristics in the presence of experimental noise and uncertainties, and the substantial variation of device properties desired. Therefore, this investigation is conducted via a thorough device simulation study.

The main advancement in the modeling of edge losses in this work is the accurate consideration of the influence of the localized edge recombination on the measurable cell characteristics. This is achieved by using the implementation of the "skin concept" in the solar cell simulation software Quokka3 [17], which enables the 3D solution of the full solar cell geometry. Here the skins represent the "near-surface" regions, which are the non-quasi-neutral regions close to the surface where e.g. a diffusion and / or a space-charge region is present. It thus intrinsically accounts for e.g. 3D semiconductor carrier transport around the edge, and the influence of the near-edge metallization geometry in conjunction with other transport-related properties like emitter sheet resistance and bulk resistivity. Such a complete description of a solar cell with edges is otherwise only possible a complex combination of detailed device simulation of the different unit cells and combining them with a distributed electrical circuit simulation [18, 19].

However, there is a fundamental limitation of the skin-concept within this context, as it cannot directly account for SCR recombination at the edge. This situation presents a truly multidimensional effect within a non-neutral region of the device, which is consequently also not addressed within the multiscale modeling approach of Quokka3, which solves skins in quasi-1D [17].

This work presents an effective solution of including SCR edge recombination within the skin-concept of Quokka3, by allowing the input of a $J_{02,edge}$ for skins bordering at specified sides, which is numerically implemented as a recombination term localized to the mesh elements next to the respective edge. This model notably differs to the commonly used "external diode model", which is hereby referred to as adding a diode representing edge recombination either within a two-diode equivalent circuit model, or as an external circuit element to a device simulation. The fundamental difference of this work's model is the consideration of the locality of the edge recombination, which correctly accounts for the influence of the limited "connection" of the edge recombination to the terminal voltage. Within 3D modeling the locality is further detrimental when also accounting for the qn-bulk edge recombination, as both mechanisms are locally coupled and can not be superimposed, as would otherwise be enforced when adding both J_{01} and J_{02} contributions within the external diode model.

In section II a "worst-case" value for the local $J_{02,edge}$ is determined by fitting Quokka3 simulations to equivalent ones using the detailed 2D / 3D device simulation tool Sentaurus Device [20] which fully resolves the SCR recombination effect.

In section III the validated model and derived $J_{02,edge}$ value is applied within Quokka3 for the 3D simulation of the full cell geometry. This 2-step approach does not impose any assumption which would disregard an important effect, and thus gives almost the same accuracy compared to hypothetically simulating the full cell in 3D resolving the SCR, which is however practically prohibitive. The impact of edge recombination on silicon solar cell performance is then investigated for a substantial variety of device properties.

Note that the investigations in this work are focused on a specific "worst-case" scenario for $J_{02,edge}$, meaning very high edge surface recombination velocities (SRVs). Restricting the investigations to this scenario is due to the fundamental SRVs for electrons S_{n0} and holes S_{p0} are usually not known both for a medium-passivated edge, which prevents a practically useful and fitting-free prediction from detailed simulations. Rather fitting the effective $J_{02,edge}$ within the skin-approach may be an easier and thus more useful approach.

II. DETERMINATION OF WORST-CASE $J_{02,edge}$

A. Simulation setup

An equivalent 2D solution domain representing the edge-region of a silicon solar cell is setup both in Quokka3 and Sentaurus for three different silicon solar cell designs: a) a typical PERC cell, b) a Fraunhofer ISE TopCon cell [21], and c) an (almost) ideal heterojunction (HJT) cell. An overview of the common solution domain is shown in Fig. 1 and a detailed list of input parameters can be found in the Appendix. Those three cell types cover already a substantial variety of properties potentially influencing edge recombination, in particular different bulk doping types and concentrations, diffused pn-junctions of both polarities and an induced pn-junction, as well as different efficiencies. In Sentaurus a region at the edge is defined around the SCR, to be able to independently set surface recombination at the quasi-neutral bulk and SCR.
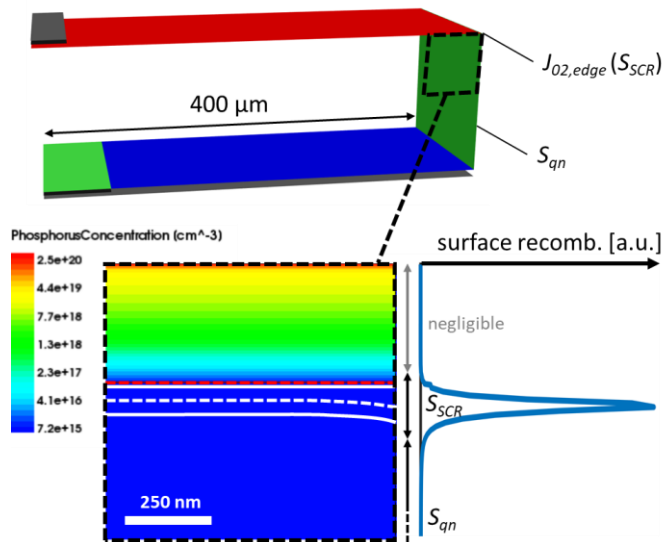

Fig. 1. Sketch of 2D edge solution domain for the PERC cell highlighting the differentiation of the two loss mechanisms; *upper*: overview as produced by Quokka3; *lower:* corner region as produced by Sentaurus, showing the phosphorus concentration (colorplot), metallurgical junction depth (red dotted line), SCR (white lines, dotted line corresponds to equal carrier densities); also plotted is an exemplary simulated surface recombination rate along the edge, showing a distinct peak at the point of equal carrier densities.

Light JV-curves (and for the PERC cell dark JV-curves) are simulated for 4 different cases: i) no edge recombination (reference case), ii) high surface recombination at the quasi-neutral bulk only (S_{qn}), iii) high surface recombination at the SCR only (S_{SCR}), and iv) both, i.e. full edge recombination. Here "high" means limited by the thermal velocity of electrons and

holes, which is assumed by setting the surface recombination velocities to $S_{n0} = S_{p0} = 10^7$ cm/s for a single defect level in the center of the band gap, and zero surface charge.

It is noted that there is no precise knowledge about the realistic values of S_{n0} and S_{p0} for an entirely unpassivated edge. Models for the thermal velocity give somewhat higher values than used here, see [22, 23]. However, the unknown degree of native passivation, and complications in transport models at such velocities (e.g. "velocity saturation"), render a precise quantification impossible, and thus a common effective value of 10^7 cm/s is used. Furthermore, a perfectly clean edge is assumed, which might not be the case in experimental reality, and thus the worst-case scenario should more precisely be considered a theoretical one, which to good approximation represents a cleanly cut edge without any passivation effect.

For the reference case of no edge recombination, consistency of input data and a very good agreement of simulation results between Sentaurus and Quokka3 is achieved. Also mesh-independency of results is ensured for both tools. In Quokka3, $J_{02,edge}$ is then varied to give the best overall agreement for all simulations including S_{SCR}.

B. Results and discussion

In Table I the main JV-parameters are summarized for the three investigated cell types, as simulated with Quokka3. For the PERC and TopCon cell the parameters with and without worst-case edge recombination of a 156mm x 156mm are shown as described in section III.For the HJT cell only the results from a unit-cell simulation are shown due to the lack of representative full-cell input parameters, explaining e.g. the relatively high J_{SC} due to the missing busbar shading.

TABLE I
QUOKKA3 SIMULATED JV-PARAMETERS OF THE INVESTIGATED CELLS

	V_{oc} [mV]	J_{sc} [mA/cm²]	FF [%]	pFF [%]	eff. [%]
PERC (156mm) *no edge recomb.*	652	39.5	79.4	83.7	20.4
PERC (156mm) *full edge recomb.*	651	39.5	78.8	83.1	20.2
TopCon (156mm) *no edge recomb.*	697	40.1	83.2	84.3	23.3
TopCon (156mm) *full edge recomb.*	696	40.1	81.8	83.1	22.8
HJT (unit cell) *no edge recomb.*	737	39.8	85.6	87.8	25.1

In Fig. 2 the edge-length specific current density loss due to edge recombination $J_{loss,edge}$ is plotted over the terminal voltage V_{term}, which is calculated by the difference of the terminal current density between the recombining case and the reference case. The SCR and qn-bulk edge recombination show a significantly different voltage dependence (ideality), but have a similar impact at and above the maximum-power-point voltage.

The results suggest that a single value of $J_{02,edge} = 19$ nA/cm can describe recombination at an exposed pn-junction largely independent of device properties and operating conditions. The value is thus specific to the semiconductor material and the edge condition assumed within the "worst-case" scenario only. This finding is supported by:

i) the entire relevant voltage range is in good agreement for all three investigated cells with substantially different properties (see Table AI);

ii) it is consistent with the simulated 20 nA/cm in [10];

iii) it was tested to be independent of additional variations of device properties (not shown): shape of doping profiles, edge domain size and metal contact position;

iv) the influence of bulk resistivity was tested by applying 10 Ωcm to all three cells (not shown): difficulties in separating SCR and qn-bulk contributions due to a largely voltage-dependent SCR size increase the uncertainty of the determined $J_{02,edge}$, but 19 nA/cm still provide a good overall agreement;

v) the position of the SCR is commonly placed within the bulk away from the varying device properties, see Fig. 1 for a diffused junction example.

Showing such a largely invariable value renders the $J_{02,edge}$ approach within the skin-concept particularly useful, as it is consequently rarely required to adjust $J_{02,edge}$ and / or redo the detailed simulations for varying device properties.

It is noted that by co-fitting the ideality factor to somewhat below 2, a better overall agreement in Fig. 2 can be achieved, which was also found in [9, 10]. This is in fact reasonable, as the SCR recombination does not take place exactly at equal carrier density, but significant recombination occurs also at significantly different carrier densities, which tends to decrease the ideality factor. However, given sufficient accuracy for most practical applications, and for the sake of simplicity and presenting a more meaningful value, it is proposed to stick to the ideality factor of 2.
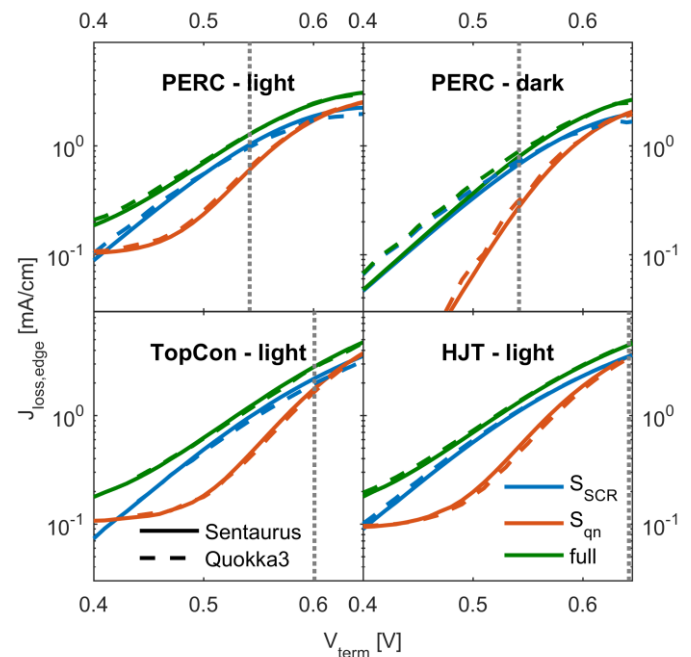

Fig. 2. Current density loss due to worst-case edge recombination as a function of terminal voltage for different solar cell designs, comparing results from Sentaurus device and Quokka3, the latter using a best-fit value of 19 nA/cm² for $J_{02,edge}$; differentiates recombination from SCR (S_{SCR}) and the quasi-neutral bulk (S_{qn}); vertical dotted lines indicate the full-cell maximum-power-point voltage.

The simulation results are also consistent with reported experimental $J_{02,edge}$ values, which show a substantial spread (5 nA/cm – 70 nA/cm, see introduction for references) but are broadly placed around 19 nA/cm. While there is a systematic difference between the experimental derived values using the external diode model and the localized $J_{02,edge}$ of this work, the differences (<50% as shown in Fig. 7) are much smaller than the spread of experimental data, and thus not invalidating the consistency. Reasons for experiments exceeding the "worst-case" simulation result could originate from extended cracks, parasitic shunts, or surface area enlargement formed by a cutting process. On the other hand, a native oxide might reduce S_{n0} and S_{p0} substantially even without applying passivation [11].

Different to the quasi-neutral bulk edge where SRV's above $\sim 10^5$ cm/s do not significantly increase the effective recombination current due to the limiting diffusion of minority carriers [6], the SCR recombination is well supplied with both types of carriers, and is found to be sensitive to S_{n0} and S_{p0} up to the thermal velocity limit, see Fig. 3. It can also be seen that for medium passivation levels, the relative influence of the quasi-neutral bulk edge is much larger than the SCR contribution, suggesting that the latter may be neglected. However, the experimental determination of both fundamental SRV values (and surface charge and defect energy levels) within the SCR is very difficult, and usually only an effective SRV value for the minority carriers is determined when characterizing a passivated surface. Therefore, such a low effective SRV cannot be simply assumed to hold within the SCR, and does consequently not exclude a high edge loss contribution from SCR recombination.

Fig. 3 also shows significant difference between the dark and the light case, meaning that superposition, which is implied by applying edge recombination as an external diode, does not hold well.
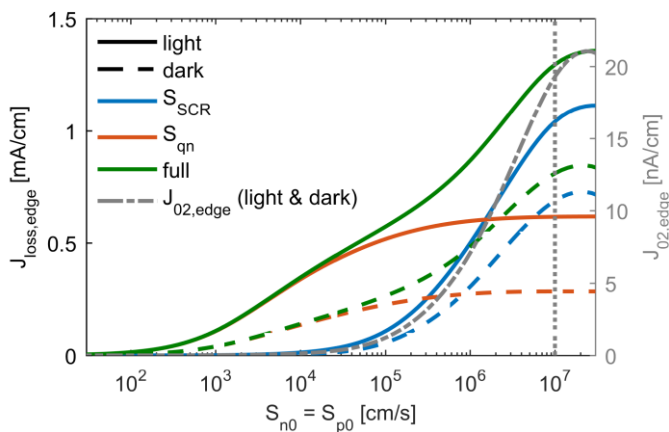

Fig. 3. Sensitivity of edge recombination loss to S_{n0} and S_{p0} (assuming zero surface charge and defect energy in the middle of the band gap) simulated with Sentaurus for the PERC 2D edge domain at a fixed voltage of 543 mV (the full cell's MPP); right y-axis and grey line additionally shows the extracted $J_{02,edge}$; vertical line indicates the worst-case assumption of this work.

III. APPLICATION TO FULL CELLS

A. Simulation setup

With the worst-case $J_{02,edge}$ value derived in the previous section, 3D simulations of 156mm x 156mm cells for the PERC and TopCon design are subsequently carried out with Quokka3, see the solution domain in Fig. 4 and input parameters in the Appendix. Still the two recombination mechanisms are differentiated, as this provides useful insight for the practical case of suppressing only one of these mechanisms by technological measures.

Light JV-curves, suns-Voc-curves (for determining the pseudo-fill-factor pFF) and for the PERC cell also dark JV-curves are simulated for all 4 edge recombination cases as defined in section II.A. The losses of individual JV parameters are then calculated by the difference to the non-recombining reference case.

Finally, for the given worst-case edge recombination case, the sensitivity of full-cell performance on device property changes are investigated by full-area 3D simulations, and compared to modeling the edge losses by the external diode to check its applicability. This is carried out via a full-factorial variation of several device properties supposed to be most influential on the cell's sensitivity on edge recombination. Those device properties comprise the cell thickness, base doping level, emitter sheet resistance, effective front and rear surface recombination as well as (asymmetric) Shockley-Read-Hall recombination in the bulk. They are varied within a broad but reasonable range, see Appendix for details. Not applying a redundant-line at the finger ends, the two types of edges are very differently connected to the metal grid and are separately analyzed, see insets of Fig. 4. Furthermore, the fundamental device design is varied as a front-junction n-type, a front-junction p-type and a rear-junction n-type cell, for the latter consequently applying $J_{02,edge}$ at the rear edges.
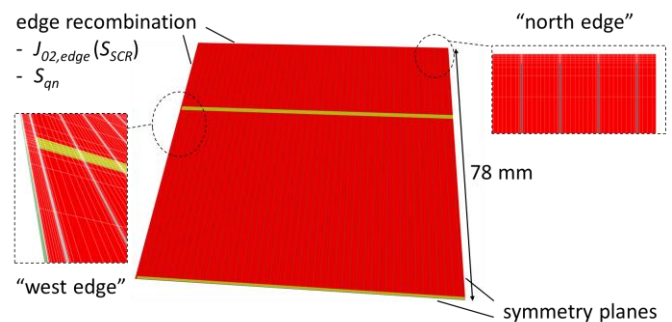

Fig. 4. Quarter solution domain of a 3-busbar PERC cell as produced by Quokka3, representing the symmetry element of a full 156mm x 156mm solar cell geometry; insets show the two different types of recombining edge geometries: "west edge" parallel to the fingers (*left inset*) and "north edge" at the finger ends (*right inset*).

B. Results and discussion

In Fig. 5 the influence of the two edge recombination mechanisms on the main light JV-parameters is shown for the two investigated cell designs. The overall losses are approximately two times higher for the TopCon cell, mainly due to the higher absolute performance. The main qualitative observations are:

i) The performance loss is dominated by a *pFF* loss, V_{oc} and J_{sc} losses are negligible.

ii) The two loss mechanisms are not additive, i.e. for a substantial reduction of edge losses the suppression of both contributions is required.

iii) While both loss mechanisms result in a similar non-ideal impact on light JV-curve, only the SCR recombination is visible in the dark JV-curve as an increased J_{02}, see Fig. 6; this means that the determination of edge losses from dark JV-curve measurements and subsequent J_{02} extraction is not suitable for the case of recombination at the quasi-neutral bulk edge being dominating.
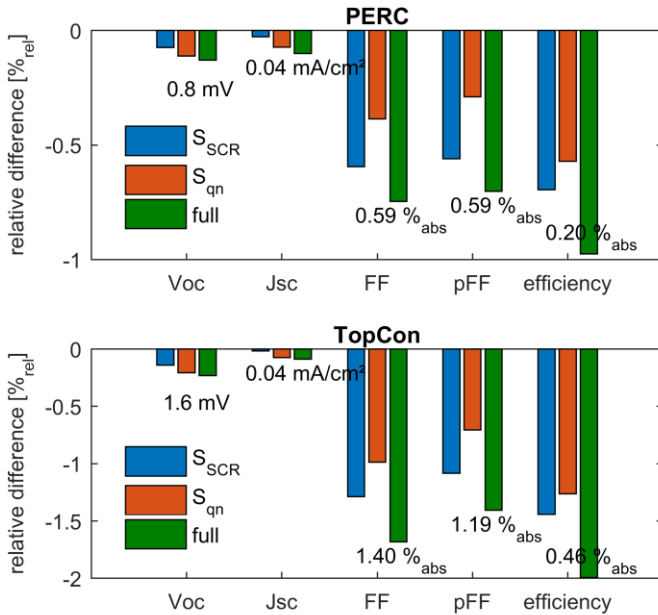

Fig. 5. Change of main light-JV parameters of full 156 mm x 156 mm cells with 4 recombining edges for the different edge recombination mechanisms; inserted values denote the absolute loss for the case of full edge recombination.
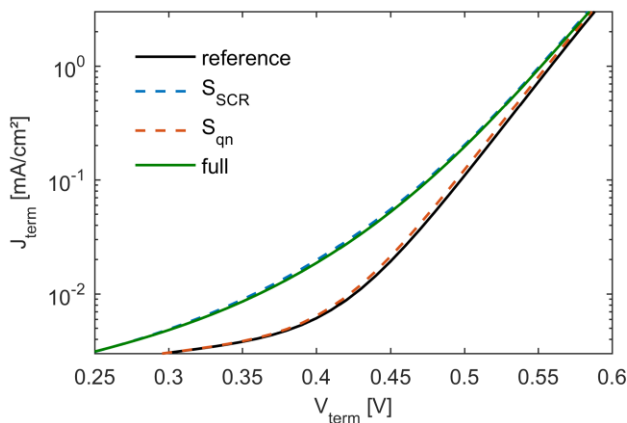

Fig. 6: Dark JV-curves of the full 156 mm x 156 mm PERC cell for the different edge loss cases; a typical external shunt resistance of 10^5 Ωcm² is assumed; solely the SCR recombination leads to an observable J_{02} increase.

The full-factorial variation of relevant device properties potentially influencing the impact of edge losses on cell performance, as detailed in Table A II, are shown in Fig. 7. The efficiency loss is plotted as a function of the series-resistance-corrected voltage, where the terminal voltage V_{mpp}, terminal current J_{mpp} and series resistance R_s are extracted from the simulation results at maximum power point. This is motivated by the edge losses represented by the second diode in the two-diode equivalent circuit model being directly correlated to this voltage. This external diode model thus appears as a unique curve in Fig. 7. It can be seen that applying the same value for $J_{02,edge}$ in the external circuit model as in the full 3D simulations, essentially assuming an ideal electrical connection of the edges to the cell's terminals and neglecting the S_{qn} contribution, the efficiency loss is predicted with a useful first-order accuracy. However, significant scatter with deviations up to 50% is observed, in particular for high voltage cells. Notably, no single device property was found to be the dominant cause for the scatter, apart from a better electrical connection via the metallization geometry leading to slightly lower losses (north vs. west edge). This means that several device properties significantly influence the cell's sensitivity on edge losses in a non-trivial way, which is not accounted for by the external diode model.

It is further noted that a change of edge-to-area ratio was investigated for few of these variation (not shown). It is found that the efficiency loss accurately scales with the edge-to-area ratio for practical cell sizes, meaning that the results shown here can well be scaled to different cell sizes.
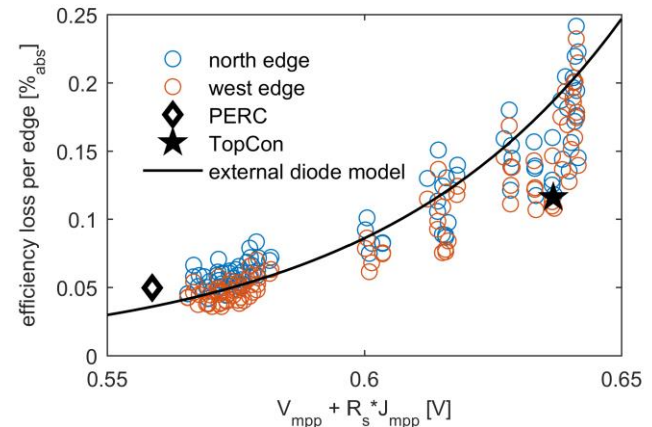

Fig. 7. Efficiency loss due to a single worst-case recombining edge in a 156 mm x 156 mm solar cell, comparing the commonly used external diode model with full 3D simulations for a full-factorial variation of several relevant device properties; also shown are the results of the PERC and TopCon full cell simulations (average values for north and west edge); the external diode model disregards some significant influence of the varying device properties.

IV. CONCLUSIONS

A new approach to model edge losses within the skin-concept of Quokka3 is introduced. Besides recombination at the quasi-neutral bulk edge, it accounts for SCR recombination due to an exposed pn-junction at the edge via a $J_{02,edge}$ property localized at the edge. With knowledge of its value, Quokka3's capabilities to solve full cell geometries in 3D can then be used to accurately model the influence on full cell characteristics.

A worst-case value for $J_{02,edge}$, representing a clean but entirely unpassivated edge, is determined by fitting to

equivalent fully detailed Sentaurus simulations for a small edge solution domain. A single value of 19 nA/cm is found to be a good approximation for a substantial variety of device properties, which is also consistent with previously reported simulations and experiments.

A subsequent large variation of device properties within 3D simulations of full cells reveal the following main conclusions:

i) The largely dominant impact of edge recombination on *pFF* as observed in previous work is confirmed.

ii) The commonly used edge loss model using an external diode does provide a reasonable first-order approximation of edge recombination caused by an exposed pn-junction. Limitations and inaccuracies arise from the fact that the assumed superposition does not hold, and in particular when predicting the influence of edge recombination for varying device properties.

iii) The quasi-neutral bulk edge recombination also leads to a similar *pFF* reduction compared to $J_{02,edge}$, is however not visible as a J_{02} increase in the dark JV-curve, and thus experimentally not characterizable by the common approach to extract J_{02} via dark JV-curve fitting.

The model of this work, next to generally providing higher accuracy and validity compared to the external diode model, will be particularly useful for non-standard scenarios. For example when investigating modifications of the edge design to suppress edge losses, see a first application to shingle cells in [24].

APPENDIX

TABLE A I
DEVICE PROPERTIES OF THE INVESTIGATED CELLS

	PERC	TopCon	HJT
cell thickness [µm]	180	200	150
number of busbars	3	5	-
busbar width [µm]	1300	500	-
finger sheet resistance [mΩ]	3.75	1.7	-
finger pitch [µm]	1700	900	-
finger width [µm]	60	24	-
front contact width [µm]	60	5	-
front contact resistivity [mΩcm²]	2	1	~0
rear contact pitch [µm]	850	-	-
rear contact resistivity [mΩcm²]	5	10	~0
front sheet resistance [Ω]	162	140	-
front J_0 noncontacted [fA/cm²]	132	10	-
front J_0 contacted [fA/cm²]	595	1800	~0
rear J_0 noncontacted [fA/cm²]	13	-	-
rear J_0 contacted [fA/cm²]	795	2	~0
bulk type	p-type	n-type	n-type
bulk resistivity [Ωcm]	2	1	1
SRH: τ_{n0} [µs] (midgap defect)	371	3710	-
SRH: τ_{p0} [µs] (midgap defect)	3710	3710	-
generation current [mA/cm²] *shading free*	42.1	41.76	40.4
lumped series resistance [Ωcm²]	-	-	0.5

Table A I summarizes the (electrical) device properties of the investigated cell designs, with the lumped skin properties as used in Quokka3. Optical effects are of minor importance in this work, and therefore only the total generation current density (exclusive of shading effects) is given here instead of more detailed optical properties.

The HJT cell was modelled using (almost) perfect a-Si properties in Sentaurus, resulting in lossless skins within Quokka3. Due to the lack of relevant input parameters, it was not simulated as a full cell, but solely as a unit cell with a (virtual) full area front and rear contact, and therefore some respective parameters are not applicable.

The parameters of the PERC cell are taken from [25], but neglecting inactive phosphorus recombination for simplicity. The TopCon cell represents typical properties for a plated metallization design as experimentally realized at Fraunhofer ISE.

TABLE A II
PARAMETER VARIATION

	lower value	upper value
cell thickness [µm]	100	200
front sheet resistance [Ω]	80	200
front and rear J_0 [fA/cm²]	10	150
bulk resistivity [Ωcm]	1	5
SRH: τ_{n0} [µs] (midgap defect)	200/2000	(no SRH)
SRH: τ_{p0} [µs] (midgap defect)	2000/200	(no SRH)

Table A II shows the parameter values as applied for the "large variation" shown in Fig. 7, which is otherwise based on the PERC cell as given above. Each parameter has a low and a high value covering a relevant range. Additionally, the bulk doping type and front and rear skin type (n-type / p-type) was varied to realize a p-type front junction, n-type front junction and n-type rear junction cell design. The SRH lifetimes with midgap energy levels were chosen asymmetric in such way that the majority carrier lifetime is 10-times the minority one for the respective bulk doping type. This full-factorial parameter variation required the simulation of ~300 light JV-curves of the full-cell domain.

V. REFERENCES

[1] R. Witteck *et al.,* "Optimized Interconnection of Passivated Emitter and Rear Cells by Experimentally Verified Modeling," *IEEE Journal of Photovoltaics*, vol. 6, no. 2, pp. 432–439, 2016.

[2] S. Zhang *et al.,* "335-W World-Record p-Type Monocrystalline Module With 20.6% Efficient PERC Solar Cells," *IEEE Journal of Photovoltaics*, vol. 6, no. 1, pp. 145–152, 2016.

[3] S. W. Glunz *et al., Eds., High-efficiency silicon solar cells for low-illumination applications*. Conference Record of the Twenty-Ninth IEEE Photovoltaic Specialists Conference, 2002, 2002.

[4] H.D.I. Gochermann and J.D.I. Soll, *Verfahren zur Herstellung eines photovoltaischen Solargenerators*: Google Patents. Available: https://encrypted.google.com/patents/DE3942205C2?cl=da.

[5] J. Zhao, A. Wang, P. Campbell, and M. A. Green, "22.7% efficient silicon photovoltaic modules with textured front surface," *IEEE Transactions on Electron Devices*, vol. 46, no. 7, pp. 1495–1497, 1999.

[6] P. P. Altermatt, G. Heiser, and M. A. Green, "Numerical quantification and minimization of perimeter losses in high-efficiency silicon solar cells," *Progress in Photovoltaics: Research and Applications*, vol. 4, no. 5, pp. 355–367, 1996.

[7] E. Franklin *et al.,* "Design, fabrication and characterisation of a 24.4% efficient interdigitated back contact solar cell," *Progress in Photovoltaics: Research and Applications*, pp. n/a-n/a, 2014.

[8]   A. Richter *et al.,* "n-Type Si solar cells with passivating electron contact: Identifying sources for efficiency limitations by wafer thickness and resistivity variation," *Solar Energy Materials and Solar Cells*, 2017.

[9]   K. R. McIntosh, "Lumps, humps and bumps: three detrimental effects in the current-voltage curve of silicon solar cells," 2001.

[10]   R. Kuhn, P. Fath, and E. Bucher, Eds., *Effects of pn-junctions bordering on surfaces investigated by means of 2D-modeling*. Conference Record of the Twenty-Eighth IEEE Photovoltaic Specialists Conference - 2000 (Cat. No.00CH37036), 2000.

[11]   M. Hermle, J. Dicker, W. Warta, S. W. Glunz, and G. Willeke, Eds., *Analysis of edge recombination for high-efficiency solar cells at low illumination densities*: IEEE, 2003.

[12]   C. Chan *et al.,* "Edge isolation of solar cells using laser doping," *Solar Energy Materials and Solar Cells*, vol. 132, pp. 535–543, 2015.

[13]   K. Rühle, M. K. Juhl, M. D. Abbott, L. M. Reindl, and M. Kasemann, "Impact of Edge Recombination in Small-Area Solar Cells with Emitter Windows," *IEEE Journal of Photovoltaics*, vol. 5, no. 4, pp. 1067–1073, 2015.

[14]   D. Bertrand, S. Manuel, M. Pirot, A. Kaminski-Cachopo, and Y. Veschetti, "Modeling of Edge Losses in Al-BSF Silicon Solar Cells," *IEEE Journal of Photovoltaics*, vol. 7, no. 1, pp. 78–84, 2017.

[15]   A. Fell *et al.,* "A detailed analysis of edge-related losses in half-cells," in *33rd European Photovoltaic Solar Energy Conference and Exhibition*, Amsterdam, Netherlands, 2017.

[16]   J. Wong, R. Sridharan, and V. Shanmugam, "Quantifying edge and peripheral recombination losses in industrial silicon solar cells," *IEEE Transactions on Electron Devices*, vol. 62, no. 11, pp. 3750–3755, 2015.

[17]   A. Fell, J. Schön, M. C. Schubert, and S. W. Glunz, "The concept of skins for silicon solar cell modeling," *Solar Energy Materials and Solar Cells,*, vol. 173, no. Supplement C, pp. 128–133, 2017.

[18]   J. Dicker, J. O. Schumacher, W. Warta, and S. W. Glunz, "Analysis of one-sun monocrystalline rear-contacted silicon solar cells with efficiencies of 22.1%," *J. Appl. Phys.*, vol. 91, no. 7, pp. 4335–4343, 2002.

[19]   G. Heiser, P. P. Altermatt, and J. Litsios, "Combining 2D and 3D device simulation with circuit simulation for optimising high-efficiency silicon solar cells," in *Simulation of Semiconductor Devices and Processes*: Springer, 1995, pp. 348–351.

[20]   Synopsis, *Sentaurus Device User Guide, release I-2013.12*. Zurich, Switzerland, 2013.

[21]   F. Feldmann, M. Bivour, C. Reichel, M. Hermle, and S. W. Glunz, "Passivated rear contacts for high-efficiency n-type Si solar cells providing high interface passivation quality and excellent transport characteristics," *Solar Energy Materials and Solar Cells,*, vol. 120, pp. 270–274, 2014.

[22]   G. Ottaviani, L. Reggiani, C. Canali, F. Nava, and A. Alberigi-Quaranta, "Hole drift velocity in silicon," *Phys. Rev. B*, vol. 12, no. 8, p. 3318, 1975.

[23]   C. Canali, C. Jacoboni, F. Nava, G. Ottaviani, and A. Alberigi-Quaranta, "Electron drift velocity in silicon," *Phys. Rev. B*, vol. 12, no. 6, p. 2265, 1975.

[24]   N. Wöhrle *et al.,* "The SPEER Solar Cell - Simulation Study of Shingled Bifacial PERC Technology Based Stripe Cells," in *33rd European Photovoltaic Solar Energy Conference and Exhibition*, Amsterdam, Netherlands, 2017.

[25]   A. Fell *et al.,* "Input Parameters for the Simulation of Silicon Solar Cells in 2014," *IEEE Journal of Photovoltaics*, vol. 5, no. 4, pp. 1250–1263, 2015.